Soil & Tillage Research 105 (2009) 12–20

Contents lists available at ScienceDirect

Soil & Tillage Research

journal homepage: www.elsevier.com/locate/still

Detection of soil water in macropores of undisturbed soil using microfocus X-ray tube computerized tomography (μCT)

Rolf Tippkötter [a,*], Thilo Eickhorst [a], Heidi Taubner [a], Beke Gredner [a], Guido Rademaker [b]

[a] Institute of Soil Science, University of Bremen, Leobener Str. UFT, 28359 Bremen, Germany
[b] Feinfocus Roentgen-Systeme GmbH, Im Bahlbrink 11-13, 30827 Garbsen, Germany

ARTICLE INFO

Article history:
Received 27 January 2009
Received in revised form 29 April 2009
Accepted 1 May 2009

Keywords:
Soil water
Computer tomography
Microscopy
Nanoparticles
Microfocus X-ray

ABSTRACT

Minimal information has been garnered regarding the spatial distribution of soil water in relation to pores and the soil matrix. Destructive layer-by-layer reconstructions derived from polished section methodology exclude any data of water in the soil. In contrast, microfocus X-ray tube computerized tomography generates images of the internal structure of the soil with a resolution down to 1 μm, at the same time creating a visual image of the spatial distribution of water in undisturbed soils.

As X-rays pass through the soil, some radiation is absorbed, some is scattered, and some is transmitted. Using advanced microfocus computerized tomography (μCT) which ensures controlled and stable output intensity for X-ray emissions and thus a constant focal spot size and spatial resolution, the resulting pattern of radiation detects to a 0.5% contrast difference. While 2D X-ray imaging is sufficient in many cases, 3D images derived from X-ray irradiation of a soil sample can reveal complex inner structures in more comprehensive format, providing information on the causal connection of water and soil structure.

Using the X-ray Feinfocus Y.FOX System and related programmes, two- and three-dimensional images of two different soils (Haplic Luvisol and Stagnic Anthrosol) at field capacity (pF 1.8) have been produced which show films of water which are associated with the pore surfaces. The mean thickness of the water films was 10.6 μm in the Stagnic Anthrosol and 3.0 μm in the Haplic Luvisol. These results were unexpected in pores >50 μm since at field capacity only the adhesive water should be present which would create water films in the range of nanometres. Myriads of colloidal dispersed nanoparticles, detected with dark field microscopy and SEM, seem to be the source of the adhesion and cohesion, causing micro-rheological effects which lead to water films of up to 30 μm in pores. Additionally, nanoparticles correlated to the clay content (fine clay) appear to conglomerate in the water films, presumably forming surface protuberances on the films of varying extent.

1. Introduction

The movement and retention of water in porous sediments in general and in soils in particular is important not only for the replenishment of groundwater, but also for the growth of plants. The subsurface transport of water, gas, and solids is linked to the soil structure, primarily to the pore spaces and to the distribution of the water in these pores. Established water energy concepts form the basic principle for describing porosity and water movement. However, only scant direct information is available regarding the pores' morphology, continuity, connectivity, and tortuosity as well as on the actual spatial distribution of soil water in relation to pores and the soil matrix.

Numerous geometrical models relating pore size distribution to soil hydraulic properties have been presented by diverse authors (e.g. Hunt and Gee, 2002; Leij et al., 2002; Tuller and Or, 2002; Dikinya et al., 2007). For the purpose of modelling the pore-scale transport processes in porous media, the Lattice–Boltzmann method (Chen and Doolen, 1998) and pore network models are frequently applied. However, these approaches require pore space geometry data for calibration and are no substitute for viewing the actual spatial arrangement of water in soils. Hence, Kutilek and Nielsen (2007) recommend a combination of hydrology and micropedology which could lead to a better understanding of the real pore and water properties in soil.

Two approaches, both based on optical techniques, may be used to produce a two- or three-dimensional or topographical representation of structural properties: (a) the destructive layer-by-layer reconstruction built up with scans or photographs taken from polished sections of resin-impregnated blocks of soil which

* Corresponding author. Tel.: +49 421 218 63450; fax: +49 421 218 7816.
E-mail address: rtipp@uni-bremen.de (R. Tippkötter).

0167-1987/$ – see front matter © 2009 Elsevier B.V. All rights reserved.
doi:10.1016/j.still.2009.05.001

have been sequentially ground down (Tippkötter, 1983) or (b) computerized tomography (CT) which generates images of internal soil structure with an in situ resolution down to 1 μm if high-resolution microfocus X-ray tube computerized tomography (μCT) is used. This method is based upon the differentiated attenuation of X-rays due to the linear attenuation coefficient which depends on both the effective atomic number and the density of the sample material. In soils, due to the substantial differences between the soil matrix and water, discrimination between these two phases is possible. With both optical approaches, the detailed image analysis is based on the same principles.

The use of CT techniques, mainly in combination with X-rays, started about two decades ago as a non-destructive means of quantifying the spatial distribution of soil properties such as bulk density or water content (e.g. Hainsworth and Aylmore, 1983; Anderson et al., 1988; Kaestner et al., 2007). Meanwhile, numerous studies were aimed at the 3D geometry of pore spaces in natural soils (Perret et al., 1999; Pierret et al., 2002) linked to soil hydraulic properties (e.g. Delerue et al., 1999; Kasteel et al., 2000; Udawatta et al., 2006). These were generally limited to the macroporosity scale (>75 μm), irrespective of technique. Generally, high-resolution μCT was applied more often when investigating 3D pore geometry or fluid flow in rocks, sediments, or model substrates such as glass beads or packed sand (e.g. Van Geet et al., 2000; Al-Raoush and Willson, 2005; Culligan et al., 2006; Lehmann et al., 2006). The potential and limitations of the different CT techniques including μCT and Synchrotron-μCT are presented by Wildenschild et al. (2002).

A successful approach to separating the water phase from the bulk soil in undisturbed soil columns was reported by Mooney (2002). The author, using a resolution of 460 μm × 460 μm × 460 μm, investigated macroporosity and water flow by comparing CT scans of samples at field capacity and after infiltration. Wildenschild et al. (2005) produced a high-resolution visualization of water in packed sand samples with pixel sizes of 17.1 and 6.7 μm, enhancing the contrast by adding potassium iodide. Adding high atomic number salts, however, changes both the surface tension and viscosity of soil water. This can be avoided by utilizing higher X-ray energies. On a small scale, the water-repellent effects of artificial hydrophobized soil aggregates were illustrated by Goebel et al. (2007) using environmental scanning electron microscopy (ESEM). Those images show water droplets and layers on soil aggregates with various contact angles (Wilhelmy plate method). Carminati et al. (2007) demonstrating the influence of hydraulic contacts between aggregates on soil hydraulic conductivity using neutron radiographs of infiltration through soil grains and synchrotron-based X-ray tomographic images of capillary bridges between aggregates.

Until now none of the aforementioned methods have been applied to detect the actual topographic location of water in undisturbed structured soils down to a microporosity scale of about 5–30 μm. The aim of this approach was to visualize the spatial distribution and the appearance of soil water in macropores (>10 μm) of undisturbed soils with digital image analysis. To this end, structured soil samples from a clayey and loess soil were investigated with microfocus X-ray tube μCT at an equilibrium water tension of pF 1.8 which represents the field capacity state.

2. Materials and methods

2.1. Soils and soil sampling

Undisturbed blocks of soil (20 cm × 20 cm) were taken from the Bv-horizon (120–140 cm) of a loess Haplic Luvisol (HL) in the southern Lower Saxony region in Germany (Banteln; 52°04′N; 9°45′E), and from the Ap-horizon (10–30 cm) of a Stagnic Anthrosol (SA; paddy soil) in the Tai-Hu region west of Shanghai in China (Jiangsu Province; 31°05′N; 120°46′E). The main properties of these soils are given in Table 1.

While the Bv-horizon (HL) is dominated by a system of continuous needle prick pores (ca. 100–400 μm) as described by Tippkötter (1983), the paddy soil (SA) has very young macropores (>50 μm), which have been created by roots of rice plants. The maintenance of the soil water content obtained at the sampling time during the transport of the soils by air or by car was ensured.

2.2. Sample preparation for CT application

The undisturbed soil samples used for X-ray CT and μCT were taken from the aforementioned soil blocks in polyvinyl chloride cylinders (12 mm in diameter; 30 mm length; 1.2 mm material thickness). A chamfer of 15° was produced in the cylinders which were wetted with water prior to sampling to provide a better penetration into the soil. As a result no disturbances of the soil structure have been observed.

The cylinders completely filled with undisturbed soil were placed uprightly on a 5 mm layer of fine silt into stainless steel soil sample rings (60 mm in diameter; 40 mm height) in order to saturate the samples using a sandbox (Eijkelkamp, Giesbeek, Netherlands). The soil was subsequently balanced to pF 1.8 by applying underpressure in the sandbox for 3 days. The cylinders were then sealed with polyvinyl chloride caps glued to both openings to prevent evaporation of soil water.

2.3. Application of microfocus X-ray tube μCT

The microfocus X-ray inspection system Y.FOX (Yxlon International Feinfocus GmbH, Garbsen, Germany; Fig. 1) used for this research consists of an X-ray source, a fixture or manipulator for the sample being inspected, and a radiation detector which includes electronics to interpret and convert the radiation incident on the detector surface into a 2D image. To create a 3D image and to cut it into digital slices, numerical, positionally precise projections must first be taken which capture the exposure pattern of the X-rays penetrating the sample at numerous orientations. The sample is rotating within the projected cone beam pattern so that a volume can be scanned all at once. It cannot be closer to the emitter than the sample radius itself. Thus, the resolution is increasing with decreasing sample size.

Table 1
Selected properties of the soils investigated.

Soil	Sand	Silt (%)	Clay	BD[a] (g cm^{-3})	TP[a] (%)	AWC[a] (%)	PWP (%)	pH $CaCl_2$	EC (μS cm^{-1})	OM (%)	CEC_{eff} (cmol$_c$ kg^{-1})	BS (%)	Fe_{ox} (mg g^{-1})
SA	0.9	58.1	41.0	1.28	51.1	13.7	34.0	4.7	149	3.30	15.6	92.7	7.30
HL	6.7	79.6	13.7	1.45	45.3	28.8	12.0	6.9	44	0.14	9.7	100	2.41

SA: Stagnic Anthrosol; HL: Haplic Luvisol; BD: bulk density; TP: total porosity; AWC: available water capacity; PWP: permanent wilting point; EC: electrical conductivity (1:5 extract); OM: organic matter; CEC_{eff}: effective cation exchange capacity; BS: base saturation; Fe_{ox}: oxalate extractable Fe.
[a] Determined with at least five cores (100 cm^3 each).

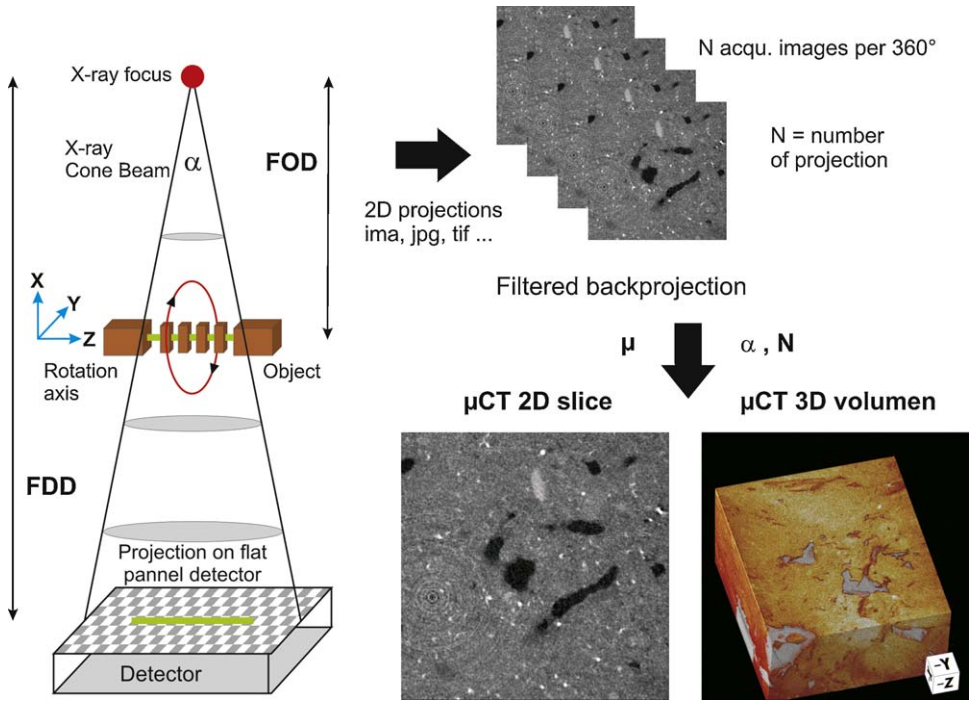

Fig. 1. Schematic illustration of an axial microfocus computed tomography system (μCT). By rotating the sample 360° in the X-ray cone beam the system acquires *N* numbers of images, called projections. The TeraRecon filtered backprojection with Feldkamp Algorithm reconstructs the μCT absorption coefficient visible in 2D oblique slice cuts or in a 3D volumen by loading all reconstructed 512 (1024, 2048 = voxel number) slices. The resulting voxel size is calculated from FOD, FDD, detector size, detector pitch, and voxel number (FOD = focus object distance, FDD = focus detector distance).

2.3.1. X-ray source

The applied multifocus tubes incorporate microfocus (1–3 μm focus), nanofocus (<1 μm focus) and high-power mode (>3 μm focus), all in one tube, providing multiple focus ranges to produce magnifications up to 2400. The potential tube energy range is between 20 kV and 225 kV, all of which are the maximum voltage for Bremsstrahlung, including the characteristic X-ray lines from tungsten. The high absorption material tungsten (W-74) is part of the exchangeable target material. In combination with a diamond (C6) supply material this target allows to accept five times more power for microfocus X-ray applications with a high resolution of less than 3 μm in 2D and 3D (Rademaker, 2005), compared to other supply materials.

The Y.FOX system includes the tube function TXI (True X-ray Intensity Control). TXI is a process that ensures controlled and stable output intensity for X-ray emission and consequently a constant focal spot size and spatial resolution. With TXI the X-ray output power on the target is stable for the whole time of the CT scan. Without precisely controlling the X-ray intensity, the reconstructed 3D image would be degraded, and may be impossible to achieve.

2.3.2. Manipulator stage

The manipulator is a high-precision CNC mechanical stage with six axes that fixes and positions the sample. The multiple axes enable irradiation at multiple oblique angles to the X-ray beam. They vary their speed of directional and rotational motion to meet specific requirements. Such speeds may range from rapid movements for quick overview searches at low magnification to very low speeds at high magnification. From an *X–Y* perspective, the range of speeds may be from 10 μm s^{-1} to 80 mm s^{-1}.

2.3.3. Detector device

The detector system is a digital 12-bit flat panel detector Varian Pax Scan 2520 with 127 μm pixel size pitch, 1–30 frames per second and a resolution of 3.94 lp (line pairs) mm^{-1}. The potential energy range extends from 40 kV to 1000 kV and can detect 0.5% contrast difference. Hounsfield (1972) introduced the computed tomography (CT) creating the Hounsfield Unit (HU) which is based on the absorption coefficient of water μ(water) and any other tissue μ(tissue). Usually a range from −1024 HU up to 3071 HU is used which covers the full range of 12-bit from the applied detector system.

All images were made with high quality (HQ) modus combined with 1888 × 1408 pixel and one frame per second. The image post-processing makes an extrapolation to 16-bit images. For image post-processing a linear contrast operator and additional noise reduction by an easy software integration function was used.

2.3.4. Measurement and data processing

The measurement time depends on the number of projections, the image quality (down to 1 μm resolution) and the noise reduction. The μCT system computationally combines all of the images to produce a 3D "reconstruction" of the original. Depending on the number of projections *N*, the image mode from the detector, and the number of slices in the reconstruction, the process time takes from 2 min (*N* = 720, HQ, 5123 voxels) to 1 h (*N* = 1440, HQ, 10,243 voxels). The slices are reconstructed by a TeraRecon cone-beam algorithm, based on a general Feldkamp reconstruction (Feldkamp et al., 1984) and pictured by i-View Workstation (TeraRecon, San Mateo, CA, USA). All reconstructed data cubes are saved in DICOM standard (Digital Imaging and Communications in Medicine).

Each image, called a projection (*N* = slice), records pixel by pixel the relative transparency or opacity of each feature imaged at a specific orientation to the X-ray source (Fig. 1). The ACT process (axial computer tomography) calculates the volume data (voxels) represented by the pixels in each slice relative to the corresponding pixels in every other slice and assigns the resulting values to a three-dimensional index according to an underlying algorithm.

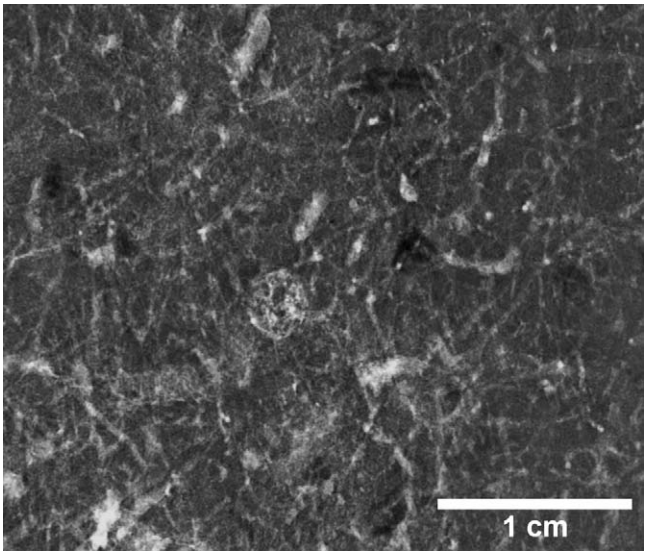

Fig. 2. X-ray tube CT-generated projection of a resin-impregnated slice of soil (Haplic Luvisol, subsoil, 10 mm in thickness) with abandoned root and earthworm channels.

Each voxel of volume data is processed until a 3D image of the sample is constructed.

2.4. Soil thin sections

Soil thin sections were basically prepared according to the method of Tippkötter and Ritz (1996). In order to preserve the biological tissues the soils were fixed with 2.5% (w/v) glutaraldehyde. They were then dehydrated with a graded series of acetone (70, 90 and three changes of 100% acetone) and maintained in 100% acetone until impregnation with polyester resin (Palatal 50-01, BÜFA, Oldenburg, Germany) which was performed under vacuum (220 mbar). After the polymerization of the resin which required 2 weeks, the cured blocks were cut into slices of approx. 10 mm thickness, polished with a grinding machine and bonded to glass slides with a polyester resin cured overnight. The bonded slices were trimmed to approx. 800 μm by cutting the slice with a diamond saw and ground to 30 μm with a lapping machine. The sections were hand-finished by lapping on glass with a diamond paste (0.75 μm) to 15–20 μm thickness. Cover slips of 170 μm thickness were bonded to the sections using a polyester resin cured within hours.

Fig. 3. X-ray tube CT-generated projection of the undisturbed soil (HL) cores used in this study.

2.5. Image analysis

Pore detection in soil thin sections and μCT-generated images is based on digital image analysis (AnalySIS 3.2, Soft Imaging,

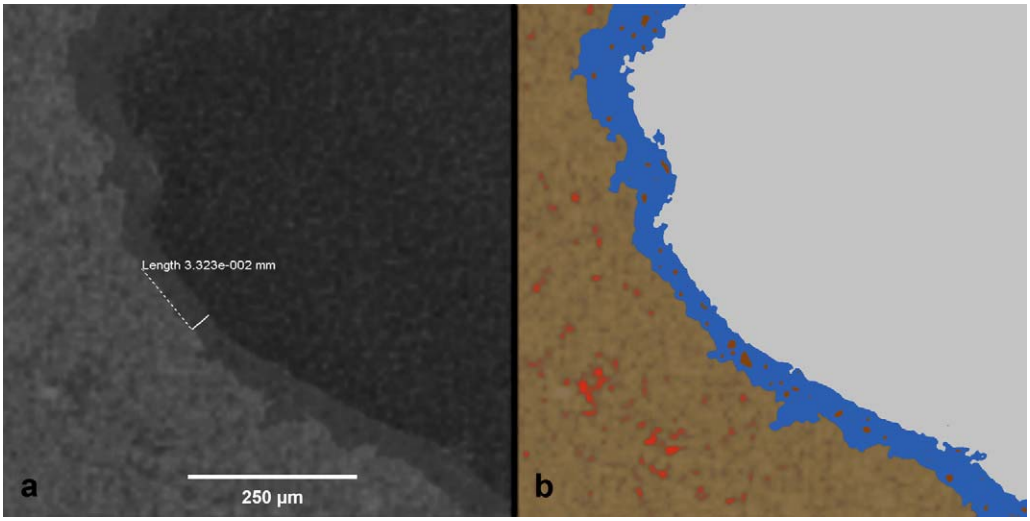

Fig. 4. μCT-generated two-dimensional section (20 μm thickness) of a macropore (Haplic Luvisol). (a) True colour (monochrome, inverted) and (b) pseudo-colour derived from the greyscale image (light grey: pore space, blue: water, brown: soil matrix).

Münster, Germany) in this paper. Different thresholds were selected for the detection of the area of the phases soil matrix, pores, and the water films. Values of pore area and perimeter were detected as well as the calculated shape factor and the equivalent circle diameter (ECD):

$$\text{shape factor} = 4\pi\left(\frac{\text{area}}{\text{perimeter}^2}\right) \quad (1)$$

$$\text{ECD} = 2\sqrt{\frac{\text{area}}{\pi}} \quad (2)$$

For the analysis of soil thin sections, micrographs taken with transmitting and polarized light were used. These micrographs were combined and calculated to one binary picture showing the area of pores. Pores in binary pictures were analysed as described above and compared with pore space data from μCT-generated images.

Equivalent areas of the pores in 2D images were calculated to classify the pore space according to the German pore size classification (Boden, 2005), i.e. wide macropores (>50 μm), narrow macropores (10–50 μm), mesopores (0.2–10 μm), and micropores (<0.2 μm).

3. Results and discussion

3.1. Preface

Many efforts have been made to characterize and visualize soil porosity using either light microscopy or CT techniques, mostly concentrated on branching intensity, morphology and tortuosity of macropores in soils. The visualization of the unaffected soil water was prevented by methodological obstacles. Making use of μCT, dark field microscopy, and scanning electron microscopy (SEM) this study presents an approach to the distribution of the unaffected soil water.

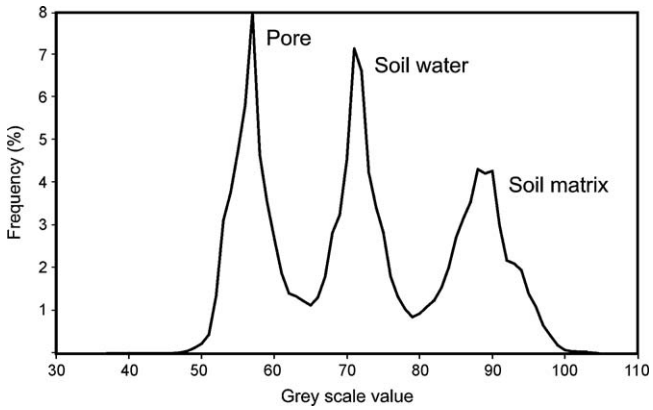

Fig. 5. Grey scale-value histogram of the phases soil, water, and air in a μCT-generated two-dimensional section.

In addition, X-ray tube CT-generated projections of undisturbed soil reveal a complex and dense network of connected tubular macropores generated by roots (Tippkötter, 1983) and earthworms, as shown exemplarily in Fig. 2.

An additional impression of the macropore architecture in undisturbed soil cores used in this study is given by an X-ray tube CT-generated projection of the filled polyvinyl chloride cylinders (Fig. 3). The projection indicates that many continuous tubular macropores are crossing this soil matrix. It also

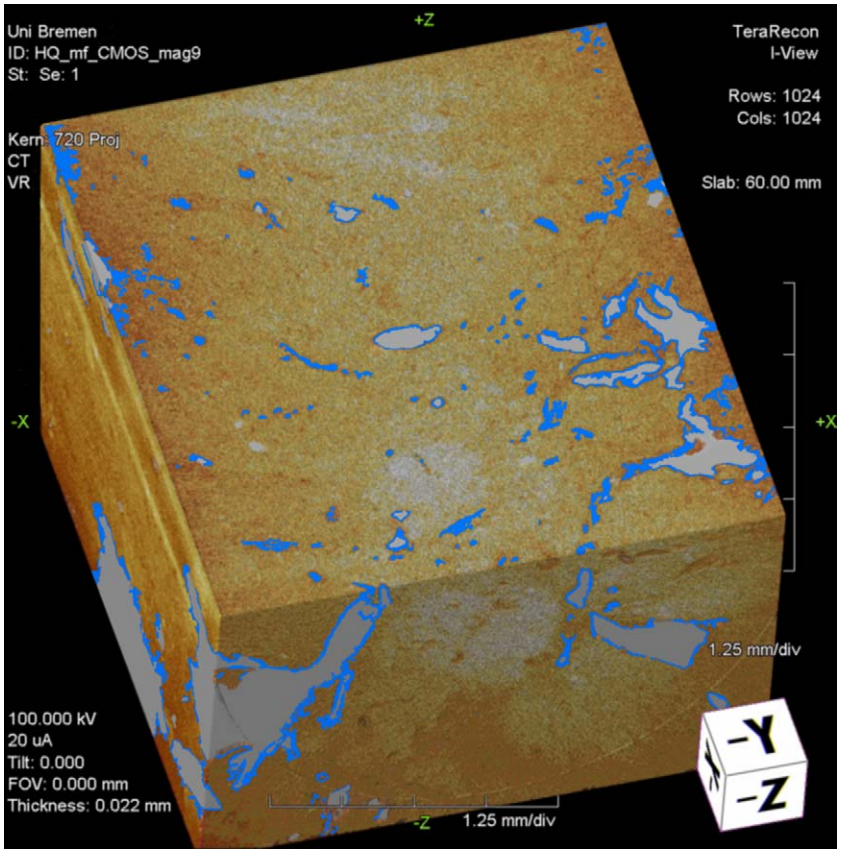

Fig. 6. μCT-generated block of an undisturbed soil (Stagnic Anthrosol) displaying the soil matrix (brown), air filled macropores (light grey) and water films (blue) at field capacity (pF 1.8).

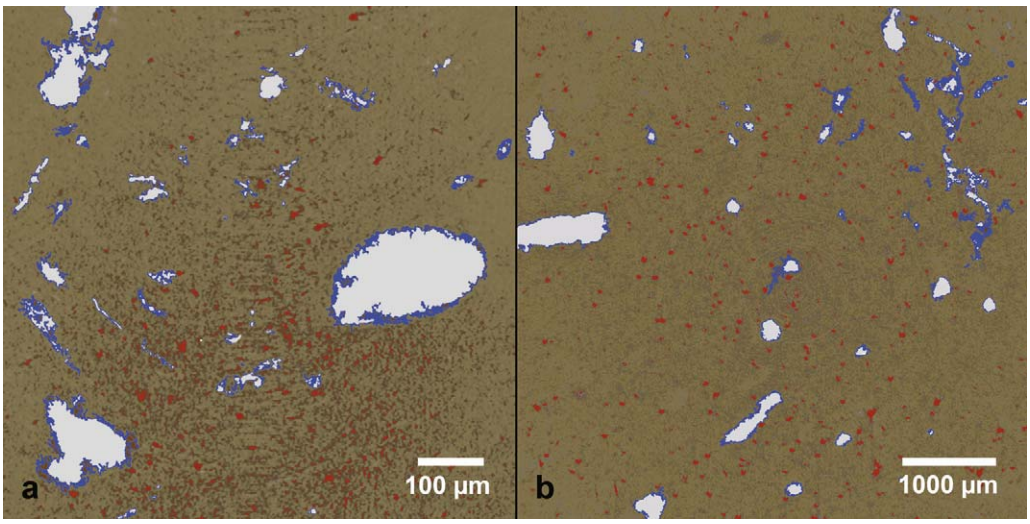

Fig. 7. µCT-generated slices (thickness 20 µm) of undisturbed soils (a: Stagnic Anthrosol, b: Haplic Luvisol) displaying the soil matrix (brown), air filled macropores (bright) and water films (blue) at field capacity (pF 1.8). Red spots indicate Fe/Mn-oxides.

demonstrates that the removal of the sample from the whole soil block did not lead to any detectable disturbances of the soil structure.

Based on the fact that the density differences between the three phases in soils are high enough, water is detectable with X-rays by its distinctive grey value signature. Due to similar densities the differentiation of water and organic matter in µCT-generated images is difficult. Nevertheless, while water displays plain and unruffled areas in the µCT-generated images, the organic matter is structured similar to chagrin paper. This rather subjectively biased classification was supported by the comparison of soil thin sections and µCT-generated images.

3.2. Application of microfocus X-ray tube µCT

Having used an X-ray tube in combination with related programmes for 2D image analyses and 3D µCT analyses of two- and three-dimensional images of two different soils at field capacity (pF 1.8), this novel approach indicates films of water which are associated with pore surfaces as shown in Fig. 4a.

The threshold modes and settings have been adjusted at the appropriate levels either automatically or manually. As shown in Fig. 5, the grey scale values of the three phases are very distinctive. This image histogram of the tonal distribution, generated with the programme AnalySIS 3.2, separates the areas of water clearly from the pore space and the soil matrix. Finally the selected areas have been coloured to match actual human perception (Fig. 4b). Although this transformation to pseudo-colour images occasionally leads to simplified values with reduced information within the regions of interest, it can make the distribution of water more obvious, by increasing the distance in colour space between successive grey levels.

A 3D impression of pore water in macropores at pF 1.8 is given in Fig. 6, showing a µCT-generated block of the Stagnic Anthrosol computed with TeraRecon i-View. Even at a low magnification films of water with different thickness have been detected in macropores at field capacity. Smaller macropores are mostly completely filled with water.

Two-dimensional sections through the µCT-generated three-dimensional matrix display a differentiated impression of the morphology of the water films in different soils (Fig. 7). The paddy soil (Fig. 7a) shows mostly young macropores of ca. 50–180 µm (mean 117 ± 48 µm) in diameter which have been caused after puddling the soil during the last vegetation period by rice roots. The loess soil (Fig. 7 b) is mainly interspersed with older tubular macropores caused by roots of cereals such as wheat and barley. Both soils correspond in the complete filling of smaller macropores (ca. <30 µm). The larger macropores show water films of different

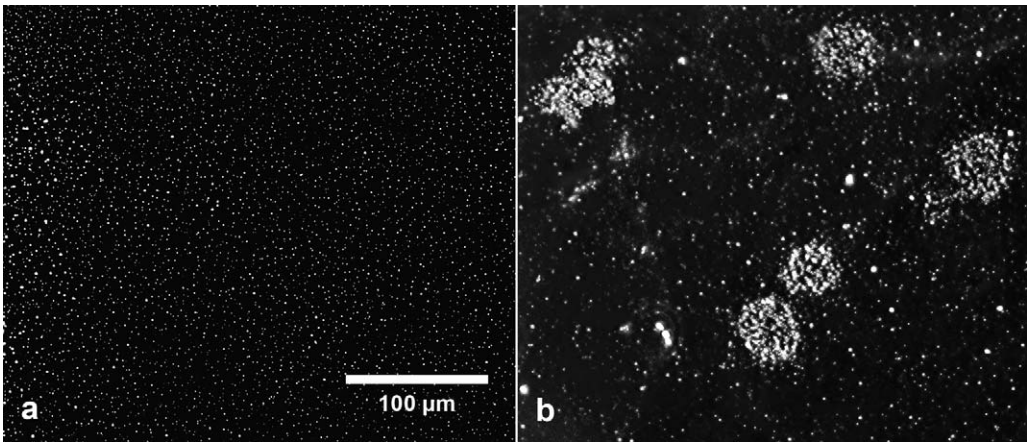

Fig. 8. Nanoparticles (mostly fine clay) in the pore water of the Stagnic Anthrosol disclosed with dark field microscopy. (a) Directly after sampling and (b) 1 h after sampling.

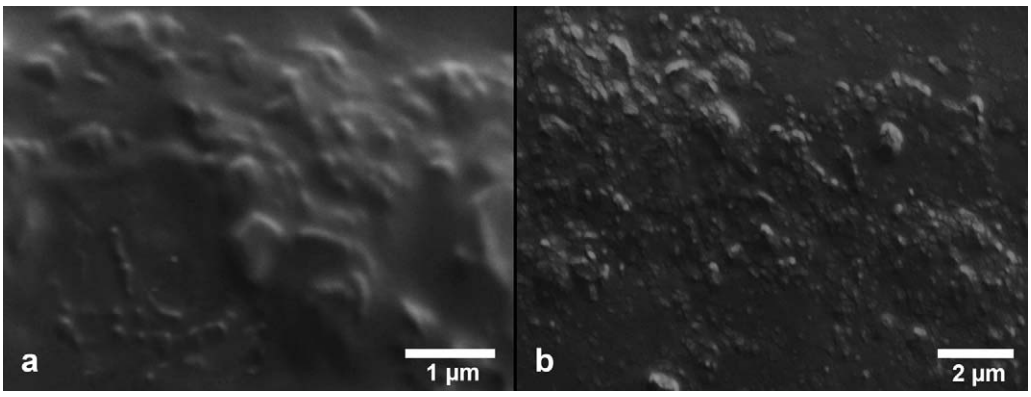

Fig. 9. Nanoparticles as shown in Fig. 8 detected with a scanning electron microscope (SEM). (a) Haplic Luvisol and (b) Stagnic Anthrosol.

thickness. The thickness of the films is, on average, at 10.6 µm in the Stagnic Anthrosol, and at 3.0 µm in the Haplic Luvisol. The biggest films found are at ca. 35 µm. These results are unexpected in pores >50 µm since at field capacity in capillary pores only water bound by adhesion should be present which causes water films in the range of nanometres. However, the variance of natural pores from the ideal capillary shape, e.g., the angular central pore space concept with corners has to be considered as a factor influencing the soil water retention (Tuller and Or, 2002).

In addition, the water films of both soils differ in shape. While the Haplic Luvisol has smooth water films, the Stagnic Anthrosol displays films with distinct protuberances. Presumably both, the outstanding thickness and shape are due to the high clay content of the Stagnic Anthrosol (ca. 40%) which leads to a high amount of dispersed mineral nanoparticles in the soil solution. It seems as if this causes strong adhesive forces promoting hydrate films on the nanoparticles initiating a non-Newtonian fluid in a rheologic system.

Microscopical investigation of the exchanged pore water of the investigated soils may explain the dynamics of the water films. Dark field microscopy reveals that myriads of nanoparticles are part of the pore water (Fig. 8). Adhesion and cohesion related to these particles could cause micro-rheological effects. A similar effect can be noticed in Fig. 4 when bigger particles (ca. 2–20 µm) of the soil matrix lead to surface protuberances on the water film. Fig. 8b indicates that the nanoparticles conglomerate under undisturbed conditions. Thus, it could be concluded that the forces of adhesion and cohesion caused by nanoparticles presumably thicken the water film of the pores.

The nanoparticles detected with dark field microscopy have been examined in detail at higher magnification with a scanning electron microscope (Fig. 9). The micrographs clearly show the hexagonal shape of clay minerals. The particle size ranges from ca. 60 nm to 1000 nm.

3.3. Image analysis

The pore size distribution of potentially detectable pores in thin sections (>1 µm) was analysed on the basis of eight micrographs of each soil. As soil thin sections were 15–20 µm thick, pores smaller than 15–20 µm cannot be determined in total. The percentage of analysed pore space was higher in the Stagnic Anthrosol than in the Haplic Luvisol (Fig. 11a). The relatively high standard deviations found are resulting from the varying orientations of the analysed cross-sections of pores. The shape factor (0 = rough and 1 = smooth) increases with decreasing pore size.

Fig. 10 shows the distribution of pores in soil thin sections after detection with image analysis. The distribution of pores in the Stagnic Anthrosol is homogeneous showing a few wide macropores and a relatively high amount of mesopores (Fig. 10a). The wide macropores result from former rice root channels (mean diameter of 173 µm). In the Bv-horizon of the Haplic Luvisol, wide and narrow macropores were detected mainly with mean diameters of 169 µm and 19 µm, respectively.

Some selected µCT-generated slices were analysed with reference to the visualized pore space and the water films. All pore size classes detected in the µCT-generated slices are within the range of the standard deviation of the pore size classes in the soil thin sections (Fig. 11a). The shape factor of these pores increased with smaller pores as it was also found in the thin sections (Fig. 11b). The shape of macropores in the Stagnic

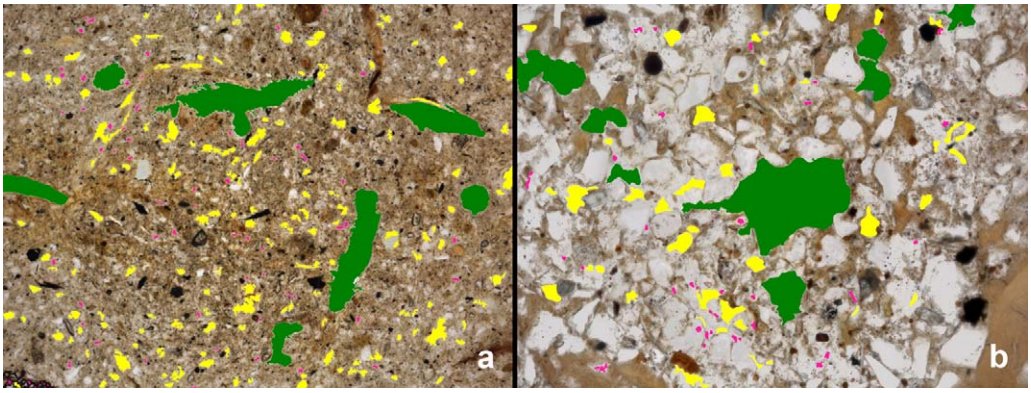

Fig. 10. Pore size analysis of the soil thin sections of (a) the Stagnic Anthrosol and (b) the Haplic Luvisol. Colourized pore space is characterizing different pore size classes. Green: wide macropores, yellow: narrow macropores, pink: mesopores. Edge length: 1100 µm. (For interpretation of the references to colour in this figure legend, the reader is referred to the web version of the article.)

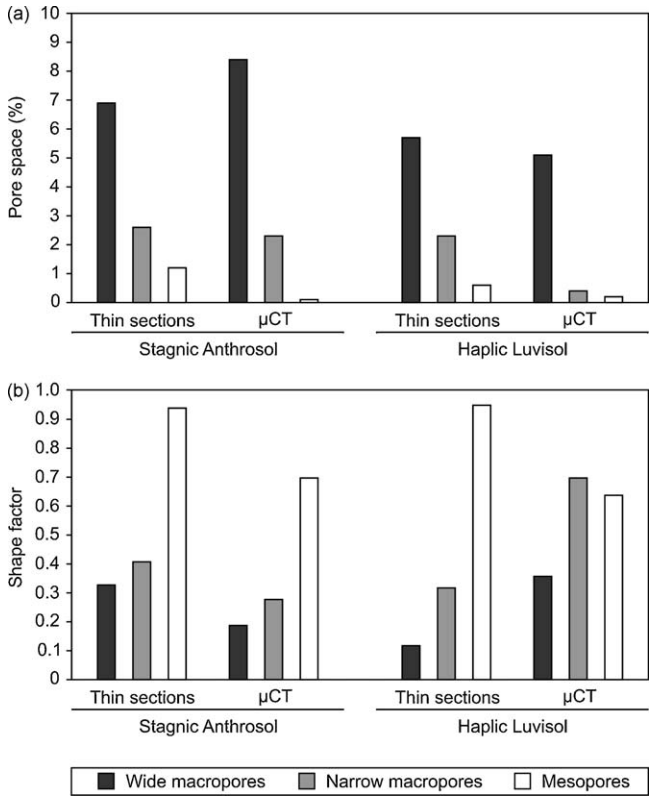

Fig. 11. Analysed pore space (a) and shape factor (b) of pores analysed in thin sections and µCT-generated images.

Anthrosol was particularly rough with values of 0.19 (wide macropores) and 0.28 (narrow macropores).

Image analysis of the water films detected in the µCT-generated images revealed that the pores of the Stagnic Anthrosol were filled with about 42% of water (52% in the Haplic Luvisol). The mean thickness of the water films was 10.6 µm in the Stagnic Anthrosol and 3.0 µm in the Haplic Luvisol. Compared to the shape factor of wide macropores (0.19–0.36), the corresponding shape factor of the water film is about two times higher (0.42 in the Stagnic Anthrosol and 0.71 in the Haplic Luvisol), indicating a smoother shape of the water film.

The detection of mesopores in the µCT-generated image of the Haplic Luvisol was limited due to a lower resolution compared to the µCT-generated image of the Stagnic Anthrosol. Micropores (<0.2 µm) were not detectable neither in µCT-generated micrographs nor in thin sections.

4. Conclusions

This study demonstrates that the localization of the distribution of natural soil water in undisturbed soil samples can be accomplished on a microporosity scale. This scale has recently been investigated with respect to the structure of soil aggregates (Peth et al., 2008), but not yet in relation to soil water.

In contrast to other investigations, natural soil samples were used instead of rock samples or model substrate media. Furthermore, it was not necessary to add contrast enhancing agents or to compare scans of wet and dry conditions (e.g. Mooney, 2002; Al-Raoush and Willson, 2005; Wildenschild et al., 2005).

The application of microfocus computerized tomography using X-ray tubes allows the visualization of both soil matrix and soil water with higher resolutions compared to speedy thermal neutrons, e.g., which have been used for the imaging of water content distribution in sand (Schaap et al., 2008).

Although water films in pores of undisturbed soil are clearly detectable in µCT-generated micrographs, open questions demand further investigations, especially in respect to the thickness of the water films and the protuberances of these films. Presumably, effects of adhesion and cohesion caused by nanoparticles are responsible for water films in the range of some micrometres in macropores. This can rather be attributed to the Stagnic Anthrosol rich in clay with water films of ca. 10 µm than to the Haplic Luvisol with only 14% clay (ca. 3 µm in thickness). In addition, the shape factor which indicates a rough surface of the water film in the Stagnic Anthrosol supports this assumption. Nevertheless, µCT has proved the hypothesis of the capillary mechanisms by displaying the capillary water in pores related to the matric potential applied: pores <50 µm in diameter were filled with water at pF 1.8 in the µCT-generated micrographs. In future the novel approach presented in this study needs to be extended to the actual soil water dynamic in smaller pores.

References

Boden, Ad-hoc-A.G., 2005. Bodenkundliche Kartieranleitung, 5th edition. E. Schweizerbart'sche Verlagsbuchhandlung, Stuttgart.
Al-Raoush, R.I., Willson, C.S., 2005. A pore-scale investigation of a multiphase porous media system. J. Contam. Hydrol. 77, 67–89.
Anderson, S.H., Gantzer, C.J., Boone, J.M., Tully, R.J., 1988. Rapid non-destructive bulk density and soil water content determination by computed tomography. Soil Sci. Soc. Am. J. 52, 35–40.
Carminati, A., Kaestner, A., Flühler, H., Lehmann, P., Or, D., Lehmann, E., Stampanoni, M., 2007. Hydraulic contacts controlling water flow across porous grains. Phys. Rev. E 76, 026311-1–026311-6.
Chen, S., Doolen, G.D., 1998. Lattice Boltzmann method for fluid flows. Annu. Rev. Fluid Mech. 30, 329–364.
Culligan, K.A., Wildenschild, D., Christensen, B.S.B., Gray, W.G., Rivers, M.L., 2006. Pore-scale characteristics of multiphase flow in porous media: a comparison of air–water and oil–water experiments. Adv. Water Resour. 29, 227–238.
Delerue, J.F., Perrier, E., Timmerman, A., Rieu, M., 1999. New computer tools to quantify 3D porous structures in relation with hydraulic properties. In: Feyen, J., Wiyo, K. (Eds.), Modelling of Transport Processes in Soils. Wageningen, The Netherlands, pp. 153–163.
Dikinya, O., Lehmann, P., Hinz, C., Aylmore, G., 2007. Using a pore-scale model to quantify the effect of particle re-arrangement on pore structure and hydraulic properties. Hydrol. Process. 21, 989–997.
Feldkamp, L.A., Davis, L.C., Kress, J.W., 1984. Practical cone-beam algorithm. J. Opt. Soc. Am. A 1, 612–619.
Goebel, M.-O., Woche, S.K., Bachmann, J., Lamparter, A., Fischer, W., 2007. Significance of wettability-induced changes in microscopic water distribution for soil organic matter decomposition. Soil Sci. Soc. Am. J. 71, 1593–1599.
Hainsworth, J.M., Aylmore, L.A.G., 1983. The use of computed-assisted tomography to determine spatial distribution of soil water content. Aust. J. Soil Res. 21, 435–443.
Hunt, A.G., Gee, G.W., 2002. Water-retention of fractal soil models using continuum percolation theory: test of Hanford site soils. Vadose Zone J. 1, 252–260.
Hounsfield, G.N., 1972. Computerized transverse axial scanning tomography. Part I. Description of the system. Br. J. Radiol. 46, 1016–1022.
Kaestner, A., Hassanein, R., Vontobel, P., Lehmann, P., Schaap, J., Lehmann, E., Flühler, H., 2007. Mapping the 3D water dynamics in heterogeneous sands using thermal neutrons. Chem. Eng. J. 130, 79–85.
Kasteel, R., Vogel, H.-J., Roth, K., 2000. From local hydraulic properties to effective transport in soil. Eur. J. Soil Sci. 51, 81–91.
Kutilek, M., Nielsen, D.R., 2007. Interdisciplinarity of hydropedology. Geoderma 138, 252–260.
Leij, F.J., Ghezzehei, T.A., Or, D., 2002. Analytical models for pore-size distribution after tillage. Soil Sci. Soc. Am. J. 66, 1104–1114.
Lehmann, P., Wyss, P., Flisch, A., Lehmann, E., Vontobel, P., Krafczyk, M., Kaestner, A., Beckmann, F., Gygi, A., Flühler, H., 2006. Tomographical imaging and mathematical description of porous media used for the prediction of fluid distribution. Vadose Zone J. 5, 80–97.
Mooney, S.J., 2002. Three-dimensional visualization and quantification of soil macroporosity and water flow patterns using computed tomography. Soil Use Manage 18, 142–151.
Perret, J., Prasher, S.O., Kantzas, A., Langford, C., 1999. Three-dimensional quantification of macropore networks in undisturbed soil cores. Soil Sci. Soc. Am. J. 63, 1530–1543.
Peth, S., Horn, R., Beckmann, F., Donath, T., Fischer, J., Smucker, A.J.M., 2008. Three-dimensional quantification of intra-aggregate pore-space features using synchrotron-radiation-based microtomography. Soil Sci. Soc. Am. J. 72, 897–907.

Pierret, A., Capowiez, Y., Belzunces, L., Moran, C.J., 2002. 3D reconstruction and quantification of macropores using X-ray computed tomography and image analysis. Geoderma 106, 247–271.
Rademaker, G., 2005. X-Ray Inspection. Whether 2-D, 3-D or both, X-ray inspection evaluates hidden features in complex devices. Qual. Digest 4, 18–24.
Schaap, J.D., Lehmann, P., Kaestner, A., Vontobel, P., Hassanein, R., Frei, G., de Rooij, G.H., Lehmann, E., Flühler, H., 2008. Measuring the effect of structural connectivity on the water dynamics in heterogeneous porous media using speedy neutron tomography. Adv. Water Resour. 31, 1233–1241.
Tippkötter, R., 1983. Morphology, spatial arrangement and origin of macropores in some Hapludalfs, West Germany. Geoderma 29, 355–371.
Tippkötter, R., Ritz, K., 1996. Evaluation of polyester, epoxy and acrylic resins for suitability in preparation of soil thin sections for in situ biological studies. Geoderma 69, 31–57.
Tuller, M., Or, D., 2002. Unsaturated hydraulic conductivity of structured porous media: review of liquid configuration-based models. Vadose Zone J. 1, 14–37.
Udawatta, R.P., Andersen, S.H., Gantzer, C.J., Garrett, H.E., 2006. Agroforestry and grass buffer influence on macropore characteristics: a computed tomography analysis. Soil Sci. Soc. Am. J. 70, 1763–1773.
Van Geet, M., Swennen, R., Wevers, M., 2000. Quantitative analysis of reservoir rocks by microfocus X-ray computerised tomography. Sediment. Geol. 132, 25–36.
Wildenschild, D., Hopmans, J.W., Vaz, C.M.P., Rivers, M.L., Rikard, D., Christensen, B.S.B., 2002. Using X-ray computed tomography in hydrology: systems, resolutions, and limitations. J. Hydrol. 267, 285–297.
Wildenschild, D., Hopmans, J.W., Rivers, M.L., Kent, A.J.R., 2005. Quantitative analysis of flow processes in a sand using synchrotron-based X-ray microtomography. Vadose Zone J. 4, 112–126.